Systematic approaches towards template-free synthesis of EMT-type zeolites

A. Nearchou, P. R. Raithby, A. Sartbaeva*

Department of Chemistry, University of Bath, Claverton Down, Bath, UK, BA2 7AY

Abstract

Presently it is understood that 18-crown-6 ether is necessary as an organic template to synthesise pure and well crystalline EMT-type zeolites. This is problematic for optimisation of organic-free synthesis of zeolites. We report a new method to synthesise pure zeolite EMC-2 using a lower amount of 18-crown-6 ether than previously reported. At these low 18-crown-6 ether concentrations, FAU-type zeolites were not seen to co-crystallise. We observe that the crystallinity of the EMT-type zeolite is proportional to the amount of 18-crown-6 ether added in the synthesis. The as-synthesised zeolites were characterised using X-ray powder diffraction, scanning electron microscopy and solid state nuclear magnetic resonance. These findings are a crucial step towards understanding template roles and designing syntheses for zeolites without the use of toxic organic templates.

Keywords: zeolite, EMT, EMC-2, FAU, synthesis, OSDA, PXRD, SEM, NMR

2010 MSC: 00-01, 99-00

1. Introduction

Zeolite EMC-2 has an EMT topology and is a hexagonal analogue of the cubic FAU framework. [1, 2, 3] Intergrowths of the two topologies have been observed widely in zeolite materials such as ECR-30, ZSM-20 and ZSM-3.[4, 5, 6,

*Corresponding Author: A. Nearchou

Email address: a.nearchou@bath.ac.uk (A. Nearchou, P. R. Raithby, A. Sartbaeva)

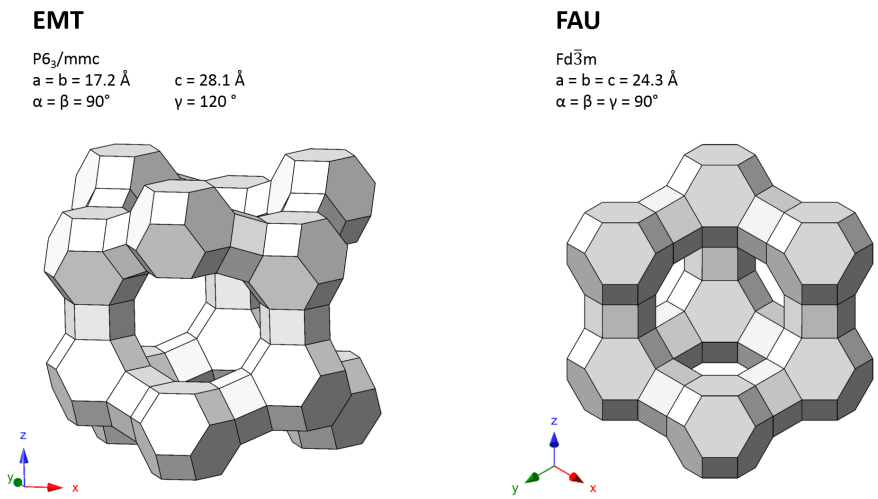

Figure 1: Idealised cell parameters [9, 10, 11] and structures of the EMT (left) and FAU (right) frameworks, with the β-cages and D6R units shaded.

7] It was not until 1990 that Delprato et al.[8] reported the successful synthesis of the pure EMT-type polymorph. This was achieved by using 18-crown-6 ether as an organic structure directing agent (OSDA).

Both the EMT and FAU framework consist of β-cages and D6R units, however the β-cages are orientated differently across the D6R units. In the EMT framework the cages are related by a mirror plane whereas in the FAU framework it is an inversion centre, as shown in figure 1. [1, 2] The two topologies are often described as hexagonal and cubic arrangements of faujasite sheets respectively. The FAU framework only contains one spherical supercage (*t-fau cage*) which has an internal diameter of 13 Å. Two different sized elliptical supercages are present in the EMT framework. The larger hypercage has an internal diameter of 13 Å by 14 Å and the smaller hypocage has a maximum diameter of 12 Å.[1] All three supercages are shown in figure 2.

The common appearance of intergrowths of the two polymorphs is believed to be due to stacking faults between these faujasite sheet layers. Treacy et al.[6] studied the distribution of stacking faults in different intergrowth FAU-

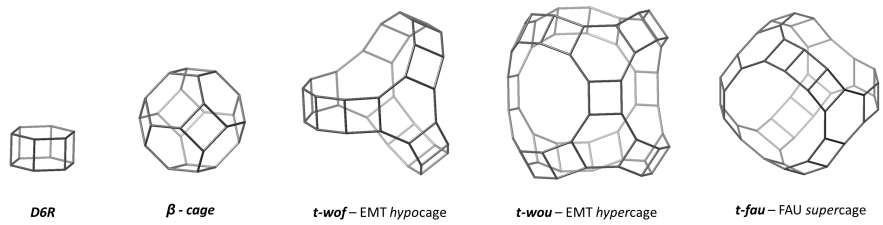

Figure 2: Structures of the building units and supercages present in the EMT and FAU frameworks.

EMT zeolite materials. It was concluded that the faults in these materials are not random, but rather segregated into discrete topological blocks. Ohsuna et al.[2, 12] have also observed the appearance of discrete blocks of either FAU or EMT-type topology in intergrowth materials.

Due to this difference in porosity, EMT-type zeolites show enhanced catalytic potential compared to FAU-type zeolites.[7, 13] However, the possibility of using zeolite EMC-2 as a catalyst is hindered by the necessity of OSDA in the synthesis process. The 18-crown-6 ether template is toxic and requires removal via calcination. Therefore, from a synthetic standpoint it is appealing to optimise the synthesis process to require less or no organic template. [13, 14, 15] This is of interest not just for zeolite EMC-2, but all zeolites synthesised using OSDA. [16, 17, 18]

Previously, pure well-crystalline zeolite EMC-2 has been synthesised using conventional hydrothermal methods with a $18C6/Al_2O_3$ ratio as low as 0.3.[1] This ratio has been reduced to 0.14 by using the SINTEF method where the hydrothermal vessel is rotated. [19] In 2012 Ng et al.[15, 14] reported the successful synthesis of ultrasmall EMT-type nanocrystals without OSDA or organic additives. This was achieved by kinetically controlling the nucleation at ambient conditions. However the product was predominantly amorphous and the nanocrystals 6-5 nm in diameter.

We report a successful new synthesis of pure zeolite EMC-2 with a $18C6/Al_2O_3$ ratio as low as 0.059 using conventional hydrothermal methods.

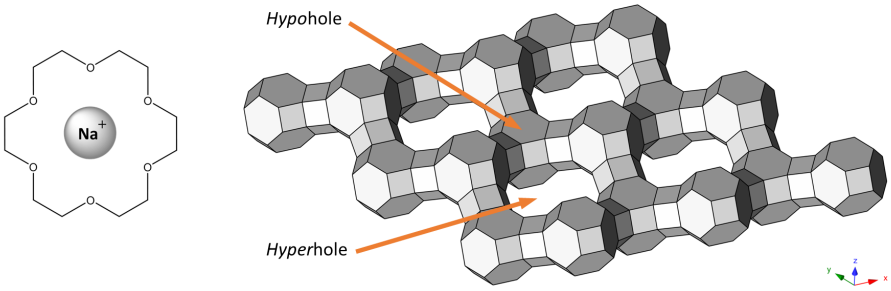

Figure 3: Diagram showing the two pockets in the faujasite sheet that the [(18-crown-6)Na^+] macrocation can occupy to form hypo- and hypercages.

2. Synthesis Mechanism

Concerning the synthetic formation of the EMT framework it is agreed that the [(18-crown-6)Na^+] macrocation complex is an integral feature. The 18-crown-6 ether molecule size, shape and ability to complex to sodium cations, are argued to be essential properties.[8, 5]

$$\frac{Na+}{[(18-crown-6)Na^+]} \tag{1}$$

Following the extended-structure approach by Feijen et al.[20] the sodium cations behave as primary cations to direct the formation of the faujasite sheets. The [(18-crown-6)Na^+] macrocation then behaves as the secondary cation and facilitates the assembly of the faujasite sheets. It does this by occupying pockets in the sheet called hypo- and hyperholes which form the hypo- and hypercages respectively,[21, 5] as shown in figure 3. There is an electrostatic attraction between the macrocation and anionic alumina in the pockets. The formation of the EMT framework is dependent on the ratio between the primary and secondary cations (equation 1). Previously we have seen the efficacy of sodium cations to assemble the FAU framework and how cation ratios are integral to understanding the synthesis mechanism of zeolites.[22]

The assembly of the EMT framework is also reportedly dependant on the Si/Al ratio of the growing structure.[21] If the hypo- and hyperholes in the faujasite sheet contain more than one alumina species, it will exceed monovalence and upon interaction with a macrocation there will be a net negative charge. Therefore additional sodium cations will be associated with the pockets for stabilisation. The presence of these cations creates a larger steric body in the hypo- and hyperholes, disfavouring the formation of the smaller hypocages. It is more sterically favourable to arrange the faujasite sheets to produce *t-fau* supercages of the FAU framework. This explains the observation that zeolite Na-X will crystallise instead of zeolite EMC-2 if the Si/Al ratio is lower than 2.6.

3. Experimental

3.1. Materials

The materials used were colloidal silica (LUDOX® HS-40, 40wt% SiO_2 suspension in water) as a source of silica, sodium aluminate ($NaAlO_2$) as a source of alumina, sodium hydroxide (NaOH) as base and a source of cation, distilled water as solvent and 18-crown-6 ether ($C_{12}H_{24}O_6$, 18C6) as OSDA. All materials were purchased from Sigma-Aldrich.

3.2. Synthesis Method

We prepared the zeolite material using a hydrothermal method analogous to that reported by Chao and Chatelain,[23] but with different proportions of precursors. The molar composition of the precursor hydrogel was $1Al_2O_3$ / $1.96Na_2O$ / $9.68SiO_2$ / x(18C6) / $87.00H_2O$, where the quantity x is varied. Samples were synthesised where: x = 0.467-0.019. The samples were referred to by the 18C6/Na_2O ratio of the precursor hydrogel. This ratio was varied 0.239-0.010.

The precursor hydrogel was prepared by dissolving the 18C6 and sodium hydroxide in distilled water. The sodium aluminate was added to the solution, and stirred until it was homogeneous. The colloidal silica was added slowly to

the solution, allowing it to gel. The resulting hydrogel was then left to incubate under stirring for 24 hours at ambient temperature. The gel was transferred to a Teflon cup inside a stainless steel autoclave and heated at 110°C for 12 days. The white precipitate crystallised from the gel was filtered and washed with distilled water until the filtrate was of neutral pH. The recovered precipitate was dried in a 100°C oven overnight. The dried powder was then ground, weighed and analysed.

3.3. Characterisation

Powder X-ray diffraction (PXRD) patterns were obtained using a Bruker D8-Advance X-ray powder diffractometer with a Cu Kα (λ = 1.5418 Å) X-ray radiation source. The unit cell parameters of the samples were calculated using the program UnitCell by Holland and Redfern.[24] The program refines cell parameters from the PXRD pattern using a non-linear least squares method.

In order to qualitatively compare crystallinity between the samples, a term called the 'ω value' was defined. This was done by deconvoluting the first three EMT framework Bragg peaks in the XRD pattern which are superimposed (2θ = 5.87 [100], 6.23 [002] and 6.65 [101]). These peaks were chosen as they are the most prominent and are observed throughout all of the indexed patterns. The area of these peaks was then calculated. The area of each peak was compared relatively to the equivalent Bragg peak of the most crystalline sample, giving a ratio. The average ratio between the three Bragg peaks was calculated, as well as the corresponding error. This ratio is the ω value, which was used to compare the degree to which EMT-type zeolite had crystallised amongst samples. The most crystalline sample was chosen as it showed the largest area for each Bragg peak. This corresponded to the sample which was synthesised using the most 18-crown-6 ether in the hydrogel (sample 1). Theoretically this should be the most crystalline sample.

Low resolution micrographs were obtained using the JEOL SEM6480LV scanning electron microcope at the Microscopy and Analysis Suite (MAS) at the University of Bath. Magic-angle spinning solid-state (MAS SS) NMR spec-

tra on the ^{29}Si, ^{27}Al and ^{23}Na nuclei were obtained using the EPSRC-sponsored Solid State NMR service run at Durham University with a Varian VNMRS 400 spectrometer. The Si/Al ratio of the zeolite samples were calculated using the following equation:

$$\frac{Si}{Al} = \frac{\sum_{n=0}^{4} I_{Si(nAl)}}{\sum_{n=0}^{4} (n/4) I_{Si(nAl)}} \tag{2}$$

Here, n is the number of adjacent aluminium nuclei and I is the relative integral intensity of each environment peak (Q^0–Q^4) after deconvolution of the spectra. Zeolite EMC-2 synthesised using the method verified by Chao and Chatelain[23] has a Si/Al ratio of 3.8.

4. Results and Discussion

4.1. Powder X-ray Diffraction Data

Table 1 lists the samples prepared with different quantities of 18C6, in addition to the hydrogel formulation ratios and the ω values. The PXRD patterns of samples 1-9 are shown in figure 4. It can be seen that as the amount of 18C6 in the gel is reduced the intensity of the Bragg peaks also decrease and the materials become increasingly amorphous. Peaks corresponding to the EMT framework are observed when the 18C6/Na_2O ratio is as low as 0.030. The PXRD patterns indicate that the samples are purely EMT-type zeolite, as no additional peaks are observed. We report that using an adjusted hydrogel formulation, synthesis of EMT-type zeolites is possible using lower quantities of 18C6 than previously reported. Before this, the lowest 18C6/Al_2O_3 ratio available to synthesise pure EMT-type zeolite was 0.14.[1, 19]

When the 18C6/Na_2O ratio is below 0.030 the samples are predominantly amorphous with low intensity peaks corresponding to the FAU framework. This suggests that there is a lower 18C6/Na_2O limit to assemble the EMT framework. Below this, faujasite zeolites preferentially crystallise, giving an EMT-FAU boundary. Previously it has been reported that rather than a distinct

Table 1: Results from decreasing the amount of 18C6 in the precursor hydrogel. All samples were run at 110°C for 12 days.

Sample	**18C6/ Na_2O**	**18C6/ Al_2O_3**	**Na^+/ [(18C6)Na^+]**	**Framework**	**ω value** *	**Max 18C6 per supercage**†
1	0.239	0.467	7.38 ± 0.004	EMT	1.00 ± 0.09	2
2	0.125	0.241	15.0 ± 0.02	EMT	0.66 ± 0.06	0.8
3	0.102	0.197	18.7 ± 0.03	EMT	0.63 ± 0.06	0.7
4	0.080	0.155	23.9 ± 0.04	EMT	0.42 ± 0.03	0.5
5	0.059	0.114	33.1 ± 0.07	EMT	0.50 ± 0.05	0.4
6	0.041	0.078	48.4 ± 0.2	EMT	0.39 ± 0.04	0.3
7	0.030	0.059	64.7 ± 0.3	EMT	0.20 ± 0.02	0.2
8	0.020	0.038	99.2 ± 0.6	FAU	-	0.1
9	0.010	0.019	199 ± 3	FAU	-	0.06

∗ A measure of PXRD pattern Bragg peak area relative to sample 1 (see Experimental).
† Estimation of the maximum number of 18C6 molecules per hypo/hypercage. Assumes that all the 18C6 molecules in the gel are integrated into the framework.

boundary, there is an overlap of the two zeolites whereby intergrowths are produced before the product is purely faujasite or amorphous.[1]

Figure 5 shows the relationship between the estimated Na^+/[(18C6)Na^+] ratio and the ω value. This supports the claims by Feijen et al.[21, 20] that the cation ratio is an integral parameter for crystallising EMT-type zeolites. The graph agrees with expectations that as the proportion of the macrocation increases so does the crystallinity of the EMT-type zeolite. From figure 5, there appears to be a negative correlation between crystallinity and the cation ratio.

The data suggests that the influence that the 18C6 molecule has on the hydrogel is dependent on its molar content. Unlike with seeding processes, it does not appear to be possible for the 18C6 molecule to form EMT-type nuclei which will spontaneously continue to grow in a hexagonal arrangement. As discussed by Ohsuna et al.[2] the 18C6 molecule is required to assemble all the faujasite sheets. Otherwise the sheets will assemble into the more thermodynamically favourable cubic FAU framework.

The unit cell parameters were refined using the peak positions and Miller Indices with the program UnitCell.[24] The results are shown in table 2. It

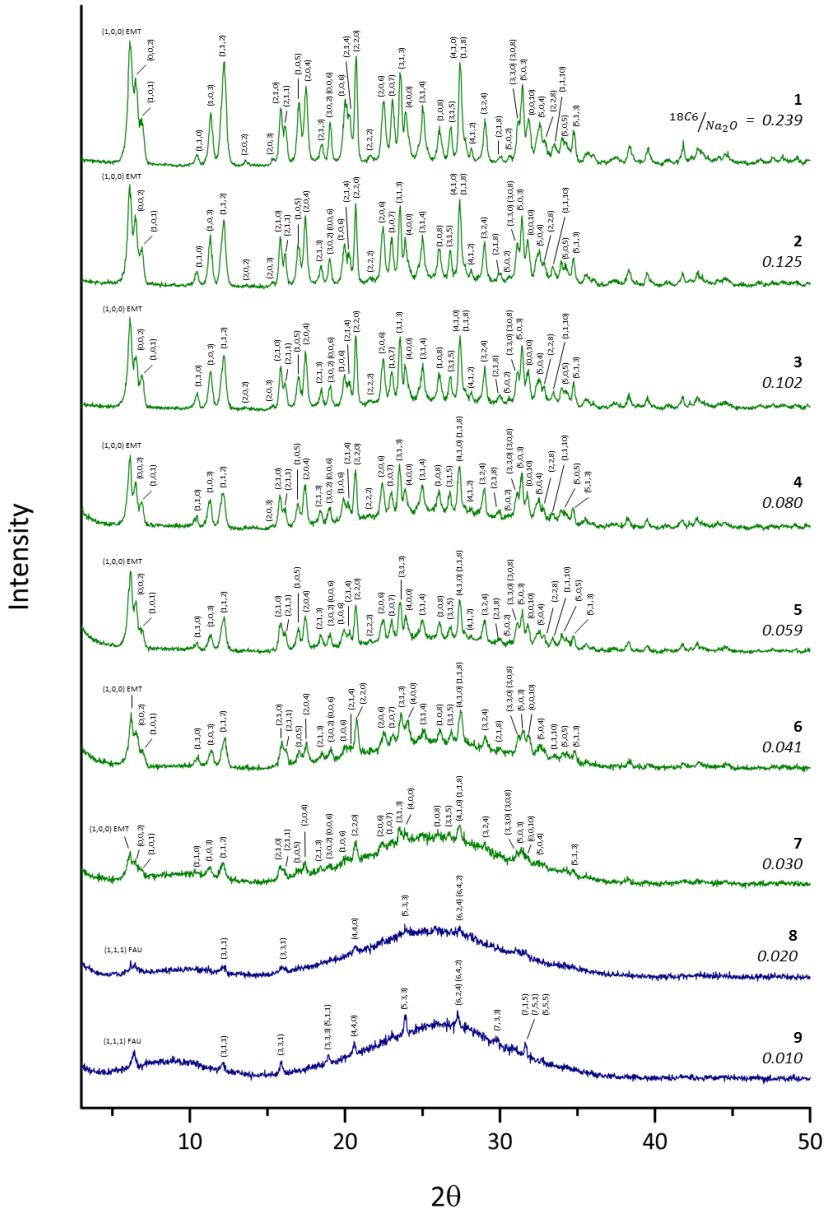

Figure 4: The PXRD patterns of samples 1-9. Values in italics are the 18C6/Na_2O ratios of the precursor gels of each sample. Green patterns are indexed to the EMT framework, and blue the FAU framework (colour online).

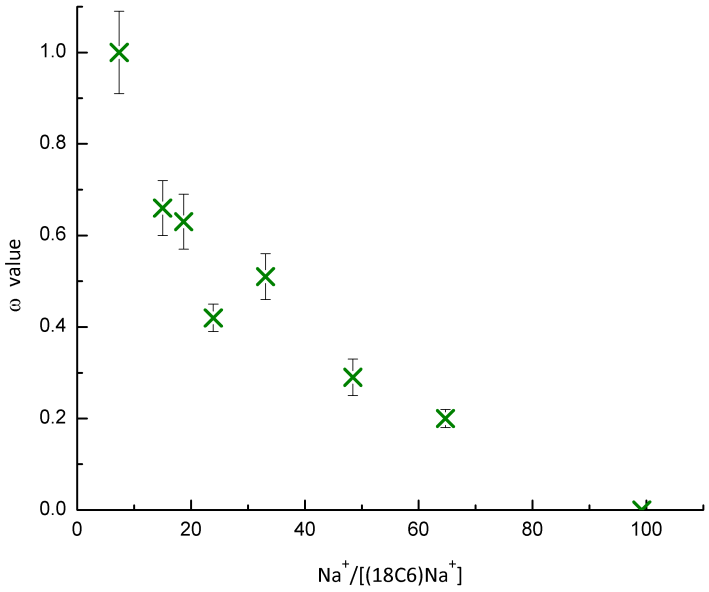

Figure 5: The relationship between the EMT-type zeolite sample ω value and the $Na^+/[(18C6)Na^+]$ ratio of the precursor hydrogel.

Table 2: Unit cell parameters of the EMT-type zeolite samples (1-7) from UnitCell.

	1	2	3	4	5	6	7
18C6/Na_2O	0.239	0.120	0.100	0.080	0.059	0.041	0.030
Unit cell parameter a /Å	17.20	17.22	17.21	17.23	17.21	17.16	17.21
Unit cell parameter c /Å	28.03	28.09	28.07	28.03	28.09	28.00	28.08
95% confidence a (x10^{-3})	1.65	1.66	1.67	1.78	1.78	1.92	2.27
95% confidence c (x10^{-3})	3.57	3.59	3.59	3.59	3.61	4.03	6.03

is clear that the decrease in 18C6 content and hence crystallinity, does not impinge the unit cell parameters. This suggests that the degree of occupancy of the supercages by 18C6 molecules does not influence the unit cell size, as we have seen from geometric simulations on the EMT framework.[25] In addition, the consistency of the unit cell paramaters implies that there is little change in the Si/Al, meaning the reduced 18C6 content does not influence Al integration into the framework.

We investigated the EMT-FAU boundary further. Samples 7 and 8, with 18C6/Na_2O ratios of 0.030 and 0.020 respectively, were repeated but with an extended hydrothermal duration of 18 days. The purpose of this was to observe whether this would lead to any thermodynamic transformations of the zeolite materials. It was expected that increased hydrothermal treatment could compensate for the limiting amount of 18C6.

Figure 6 shows the PXRD patterns of samples 7 and 8 compared to the repeats with extended duration of hydrothermal conditions. The patterns indicate that with a low 18C6/Na_2O ratio of 0.030 (sample 7b) the crystallinity of the EMT-type zeolite could be enhanced by increasing the hydrothermal duration. This confirms that the EMT framework can be assembled at the low boundary of 18C6 given longer crystallisation time. The repeated synthesis using an 18C6/Na_2O ratio of 0.020 (sample 8b) was amorphous after 18 days of hydrothermal conditions. In figure 4 peaks corresponding to the FAU framework were observed in the PXRD pattern of the highly amorphous material. This suggests that at low 18C6 contents, the hydrogel does not intrinsically favour the assembly of the FAU framework.

4.2. SEM Micrographs

Figure 7 shows SEM micrographs of samples 1 and 8, demonstrating the coherent difference in morphology when decreasing the 18C6 content. Sample 1 in micrograph 7a shows hexagonal platelet structure, which is typical of EMT-type zeolites. The hexagonal shapes have smooth corners, which contrasts the sharpness which is usually observed.[2, 8] Viewing the particles perpendicular

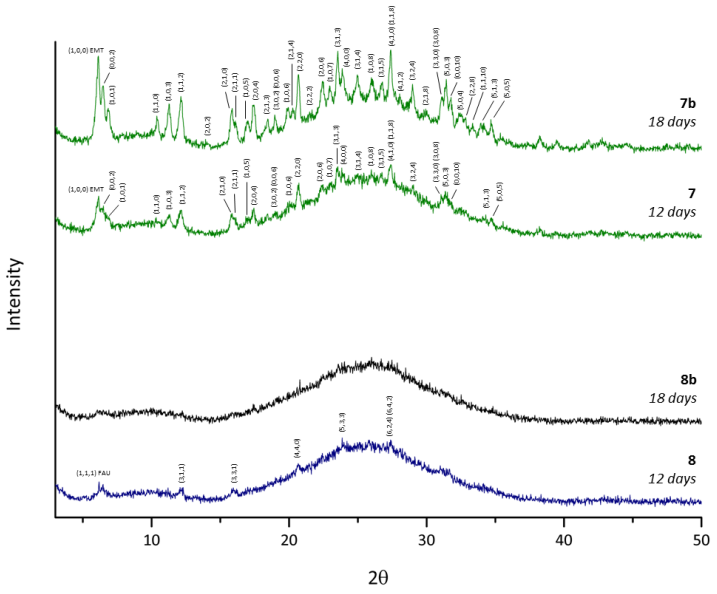

Figure 6: The PXRD patterns of samples 7, 7b, 8 and 8b. Samples 7 and 7b have the same hydrogel formulation, as did 8 and 8b. b indicates the extended duration of hydrothermal conditions from 12 days to 18 days. Green patterns are indexed to the EMT framework and blue the FAU framework (colour online).

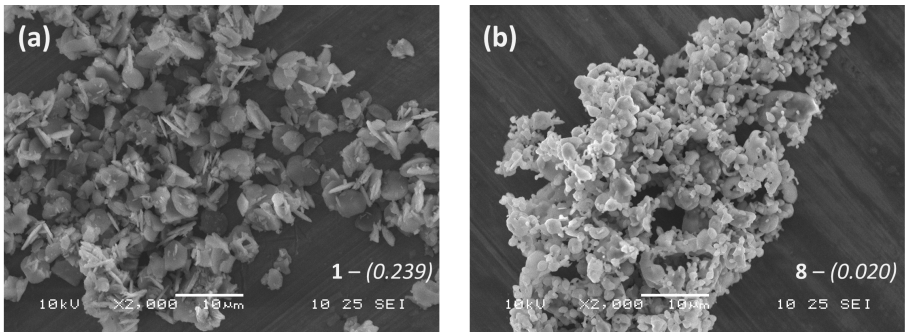

Figure 7: SEM micrographs on the 10 μm scale showing the contrast in morphology. Micrographs a) Sample 1, 18C6/Na_2O = 0.239, EMT and b) Sample 8, 18C6/Na_2O = 0.020, FAU/Amorphous.

to the c axis, it can be seen that the platelets are rounded in a sense to give a pointed edge. We described this as flattening of the platelet edge. Sample 8 was shown to be predominantly amorphous from PXRD, and micrograph 7b corroborates this. The hexagonal platelet morphology is absent and instead there appears to be a distribution of ellipsoids lacking any regular features. Although weak Bragg peaks corresponding to the FAU framework were observed in the PXRD pattern, no octahedron shape crystals can be seen by SEM, confirming the absence of crystalline FAU-type zeolite.

SEM micrographs on the 5 μm scale are shown in figure 8. The micrographs illustrate the morphology transition from hexagonal platelets to amorphous ellipsoids. Micrographs 8a and 8b show samples 1 and 3, respectively. Comparison between these two images shows that the hexagonal platelets become thicker when the amount of 18C6 in the synthesis gel is reduced. This pattern continues in sample 5 (figure 8c) where the platelets are thicker than sample 3. This is confirmed by particle size analysis, as shown in figure 9. In addition to this, the platelets appear to have a uniform thickness as opposed to flattened edges as was seen in sample 1. The thickening of the platelets with reduced 18C6 suggests promoted growth along the [001] direction.

Dhainaut et al.[26] also observed thickening of the hexagonal platelets. When 1,4-di(azo-18-crown-6 ether)-butane (AC6-4) was used as OSDA to crystallise

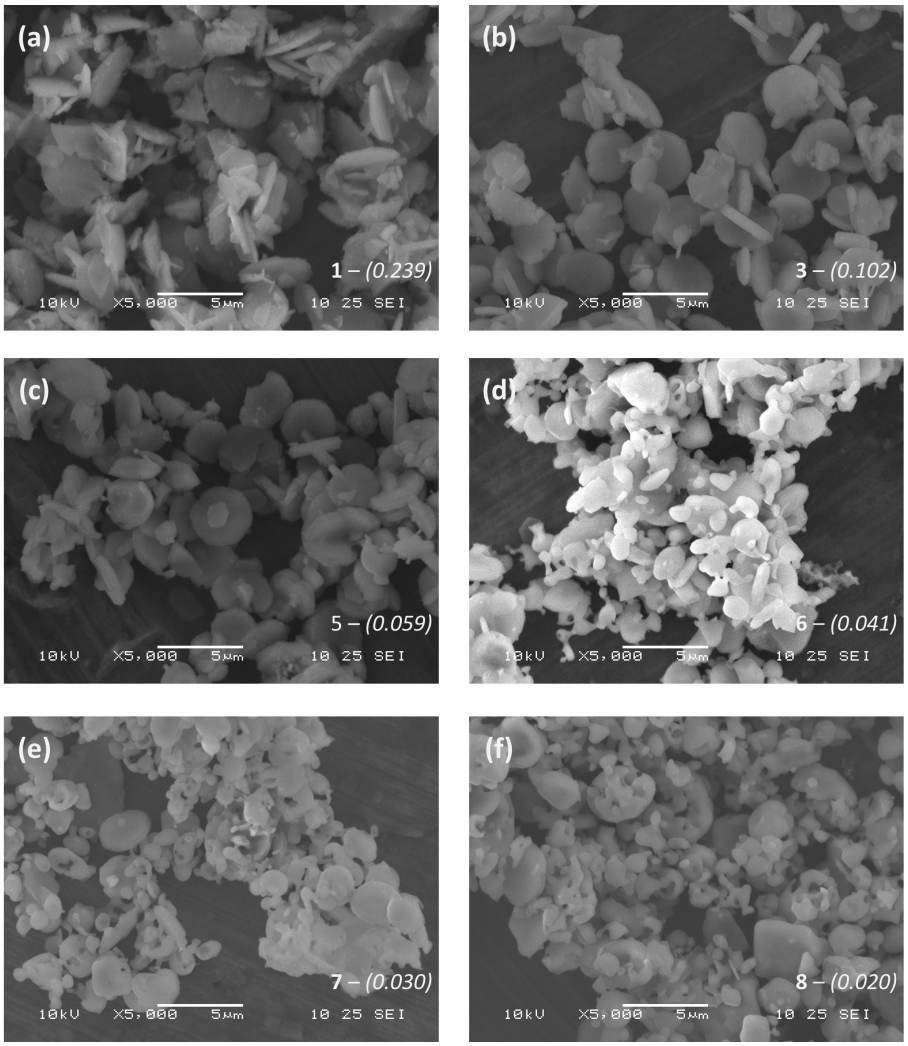

Figure 8: SEM micrographs on the 5 μm scale showing the change in morphology with 18C6 content. Micrographs a) Sample 1, 18C6/Na_2O = 0.239, EMT, b) Sample 3, 18C6/Na_2O = 0.102, EMT, c) Sample 5, 18C6/Na_2O = 0.059, EMT, d) Sample 6, 18C6/Na_2O = 0.041, EMT, e) Sample 7, 18C6/Na_2O = 0.030, EMT and f) Sample 8, 18C6/Na_2O = 0.020, FAU/Amorphous.

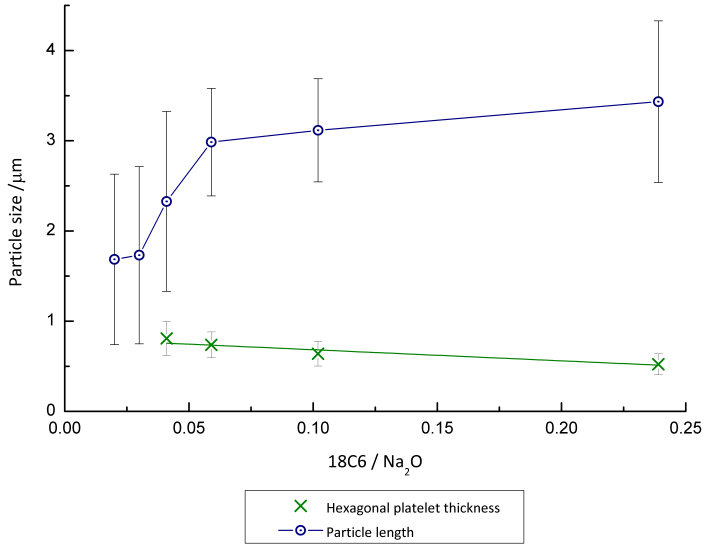

Figure 9: The variation in particle size with the 18C6/Na_2O ratio of the precursor gel. Measurements taken from the SEM images. The green crosses show the average hexagonal platelet thickness, and the blue circles show the average particle length.

zeolite EMC-2 the platelet crystals were smaller and thicker compared to using 18C6. It is interesting to note that the crystallinity was reduced to 60% when using AC6-4 instead of 18C6 as OSDA. In conjunction with our results, this suggests a relationship between crystal thickness and crystallinity based on the efficacy of the OSDA to direct the EMT framework.

The hexagonal morphology appears to become more similar to circular discs with reduction of 18C6 in the hydrogel. This smooth disc morphology has been seen by Wendelbo et al.[1] where EMT-type platelets were synthesised at 18C6/Al_2O_3 contents of 0.206 using the SINTEF method. This 18C6 content is greater than sample 5, which shows hexagonal platelet morphology (figure 8c) with a 18C6/Al_2O_3 ratio of 0.114.

Sample 6 onwards, the hexagonal and disc morphology is lost as shown in micrographs 8d, 8e and 8f. These are the samples where the 18C6/Na_2O ratio was below 0.059, 18C6/Al_2O_3 below 0.114 and the ω valuey below 0.42.

These samples appear to be highly amorphous, showing the random ellipsoid morphology. PXRD of samples 6 and 7 indicated the presence of EMT-type zeolite, however the morphology appears amorphous. Both samples 8 and 9 were identified as being highly amorphous, so it is not surprising to see a lack of crystalline shape.

It is interesting to see that there appears to be a jump in morphology between sample 5 (figure 8c) and sample 6 (figure 8d). It is between these two samples that the hexagonal/disc morphology is lost and the material appears predominantly amorphous. This suggests that although the EMT framework can assemble there is an 18C6 limit to produce defined platelet crystals.

From figure 9 it can be seen that as the 18C6/Na_2O ratio decreases the length of the particles seen in the SEM micrographs decrease. However, the size of the errors bars indicate that there is a substantial spread in the size of the particles produced, as can be seen in the micrographs.

4.3. Solid State NMR

Solid State Magic Angle Spinning NMR data were collected using the ESPRC-run NMR National Facility at Durham University.

4.3.1. ^{29}Si NMR

The ^{29}Si SS MAS NMR of the samples that were observed by SEM analysis are shown in figure 10. Assignment of the peaks was performed following Lippmaa et al.[27], with only samples 1, 3 and 5 showing enough coherence for confident assignment. These three spectra show four resonances at approximately -106, -100, -95 and -89 ppm which correspond to the Q^4, Q^3, Q^2 and Q^1 environments, respectively. These are listed in table 3. As the samples become increasingly amorphous the coherence between the different silicon environments is lost.

The calculated Si/Al ratios of the crystalline samples are also shown in table 3. These Si/Al ratios agree with what is typically expected of EMT-type zeolites.[21, 23] There does not appear to be any consistent pattern between

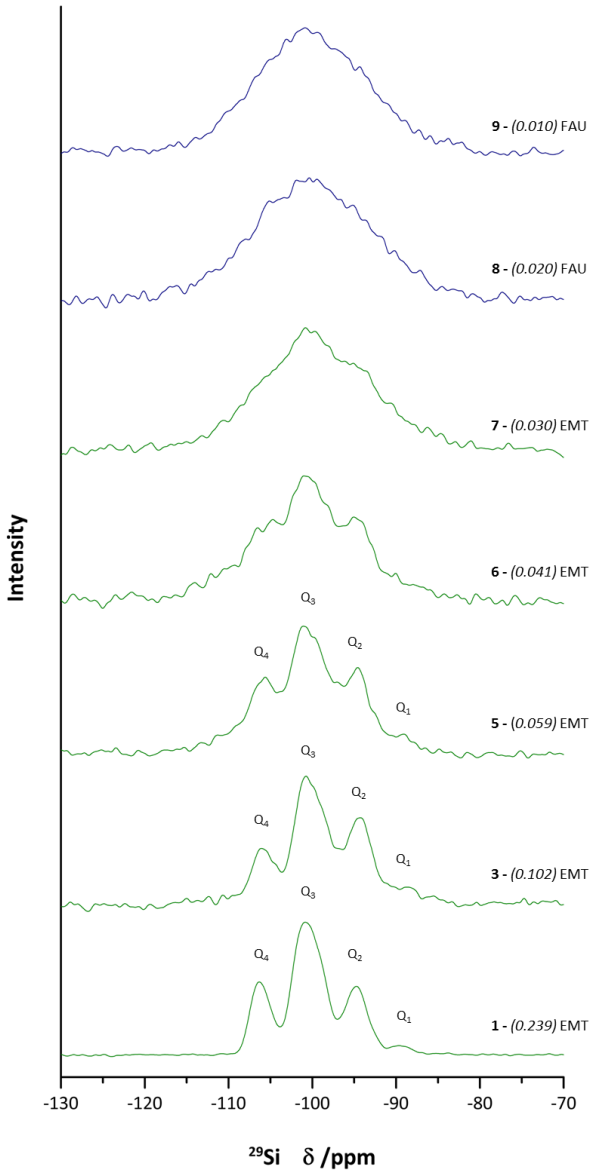

Figure 10: SS MAS NMR spectra for the ^{29}Si nuclei for samples 1, 3, 5-9. The values in italics indicate the 18C6/Na_2O ratio of the precursor hydrogel in each sample. Green spectra correspond to EMT-type zeolites and blue FAU-type (colour online).

the amount of 18C6 in the hydrogel and the Si/Al of the crystallised zeolite. This suggests that the presence of OSDA does not have a major influence on the amount of aluminium being integrated into the growing framework.

Previously Feijen et al.[21] argued that the amount of aluminium in the framework could not exceed a monovalence per pocket in the growing faujasite sheets. This was based on the sterics of the 18C6 macrocation and additional sodium cations sitting in the pocket. Therefore, it was the presence of the 18C6 molecule in each supercage constraining the Si/Al ratio. However, we have shown that despite decreasing the number of 18C6 molecules per supercage available there is not a large impact on the Si/Al ratio.

4.3.2. ^{27}Al NMR

Figure 11 shows the ^{27}Al SS NMR spectra of samples 3, 5-9. Only resonances positioned between 61-55 ppm were observed, which is consistent with a tetrahedral arrangement. [28] The chemical shift of the maxima of each peak is reported in table 4. It can be seen that as the sample becomes increasingly amorphous the resonance moves to a lower chemical shift. However, the spectra for samples 5-7 show visible shoulders due to the presence of the resonance at approximately 55 ppm, seen in the more amorphous samples. This suggests that there are two tetrahedral ^{27}Al nuclei environments.

Table 3: Chemical shift (δ/ppm) and type of silicon environments present from ^{29}Si SS MAS NMR spectra for samples 1, 3 and 5. Si/Al ratio calculated for the samples using equation 2 and the intensity integrals from each of the silicon environments.

	1	**3**	**5** †
Q^4 /ppm	-106.3	-106.1	-106.2
Q^3 /ppm	-100.5	-100.3	-100.5
Q^2 /ppm	-94.7	-94.5	-94.8
Q^1 /ppm	-89.6	-88.9	-89.2
Si/Al Ratio	3.85	3.29	3.46

† Indicates that the spectrum fit using deconvolution was not ideal due to background noise.

Table 4: Peak positions in the ^{27}Al SS MAS NMR with different 18C6 contents for samples 3, 5-9.

	3	**5**	**6**	**7**	**8**	**9**
^{27}Al δ /ppm	60.6	60.1 *	59.9 *	54.9 *	54.4	55.1

$*$ Indicates that the peak has a shoulder

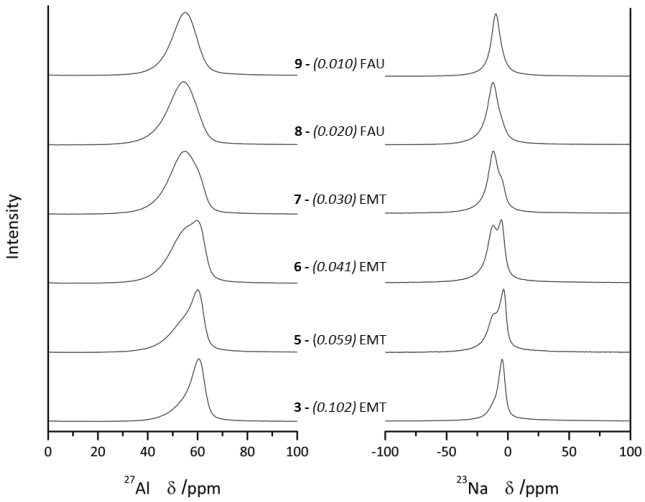

Figure 11: SS MAS NMR spectra for the ^{27}Al nuclei (left) and ^{23}Na nuclei (right) for samples 3, 5-9. The values in italics indicate the 18C6/Na_2O ratio of the precursor hydrogel in each sample.

Table 5: Peak positions in the ^{23}Na SS MAS NMR with different 18C6 contents for samples 3, 5-9.

	3	**5**	**6**	**7**	**8**	**9**
^{23}Na δ /ppm	-4.63	-3.42	-5.35	$*$		
		-10.9	-11.8	-11.6	-12.1	-9.91

$*$ Indicates that the peak has a shoulder and the exact position cannot be resolved.

4.3.3. ^{23}Na NMR

The ^{23}Na SS NMR spectra show a pattern similar to that of the ^{27}Al nuclei (figure 11). There appears to be a switchover of two different environments. The two resonances are observed at approximately -4 ppm and -11 ppm. The peak positions for each sample are listed in table 5. The extra framework sodium cations will be positioned to charge balance the anionic alumina sites in the framework. Therefore it is likely that the shift in resonances observed in the ^{23}Na nuclei spectra is a consequence of the change in ^{27}Al environments as the 18C6 content decreases.

Observations by Hunger et al.[29] using ^{23}Na MAS NMR on an EMT-type zeolite indicated that there are two resonances at -7 ppm and -11 ppm. These corresponded to three cation sites in the framework, as shown in figure 12. However, this does not directly correspond to the data we have obtained, suggesting that the sodium cations are sitting in different positions. Later ^{23}Na NMR spectroscopic analysis by Feuerstein et al.[30] on zeolite NaX showed resonances at -4 ppm and -12 ppm, with the former being quite similar to what we observed experimentally. The resonance at -4 ppm for zeolite NaX was identified as sodium cations positioned inside the β-cage, close to a D6R unit. This is similar to the cation site S1$'$ shown in figure 12 in the EMT framework. Both Hunger et al.[29] and Feuerstein et al.[30] agree that the higher resonance around -11 ppm corresponds to sodium cations sitting in the framework supercages, close to the 6 ring face of a β-cage. However, this resonance has also been ascribed

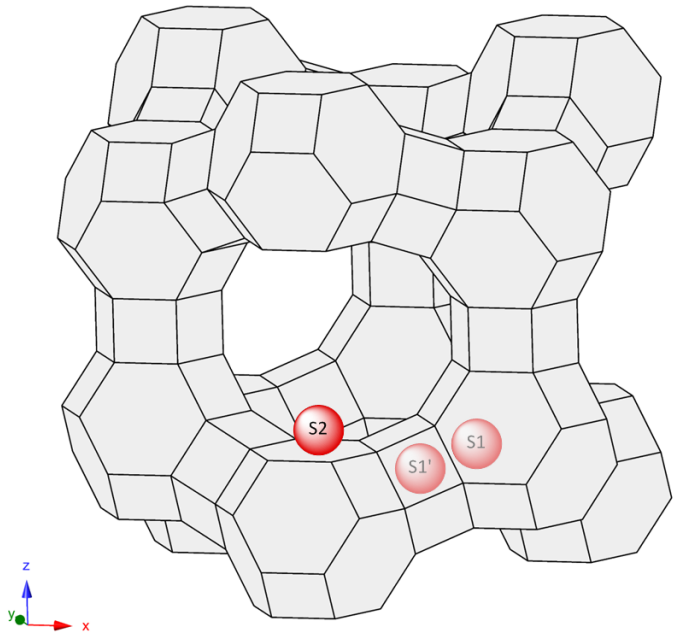

Figure 12: The three positions in the EMT framework occupied by sodium cations, as described by Hunger et al. using ^{23}Na MAS NMR. [29]

to sodium cations siting within the D6R units in zeolite NaX. Therefore, the resonance at -11 ppm we have observed can be identified to sites S2 and S1 in the EMT framework, shown in figure 12. Considering that the position of this peak varies; it is possible that the population of these two sites change with 18C6 content.

5. Conclusion

We have successfully synthesised pure EMT-type zeolite using a lower molar quantity of 18C6 than previously reported, using an adjusted hydrogel composition. Hexagonal platelet crystals of EMT-type zeolite were synthesised with a 18C6/Al_2O_3 ratio of 0.114 and a 18C6/Na_2O ratio of 0.059. PXRD data indicated that these ratios could be reduced to 0.059 and 0.030 respectively, and still show presence of an EMT topology. However the morphology appeared spherical and non-uniform at such low 18C6 contents. This suggests that under these synthesis conditions, a minimum of 0.2 18C6 molecules per supercage are required in the hydrogel to assemble the EMT framework. FAU-type zeolites were not observed to cocrystallise alongside EMT, but appeared below the 18C6/Na_2O threshold of 0.030. We have also shown that despite the low crystallinity of the EMT-type zeolite at these low 18C6 contents, extended hydrothermal treatment can be used to produce a more crystalline material.

SEM analysis showed that the hexagonal platelets got thicker as the 18C6 content in the hydrogel decreased. This suggests that increasing the content of 18C6 disfavours particle growth along the c axis.

Reducing the 18C6 also appears to lower the chemical shift of the ^{27}Al nuclei resonance in the SS NMR, while remaining in a tetrahedral environment. It also appears to significantly alter the occupancy of sodium cation sites in the framework. When the 18C6/Na_2O ratio was lower than 0.059 the coherence of the ^{29}Si NMR spectra was lost due to a large degree of amorphous content. The Si/Al ratio of the crystalline samples above this threshold were between 3-4, typical of EMT-type zeolites.

Overall we have shown that EMT-type zeolites can be produced using less 18C6, approaching a more sustainable and environmentally cleaner synthesis.

Acknowledgements

A.S. thanks the Royal Society for funding. P.R.R. and A.N. thank the EPSRC for funding (grant number EP/K004956/1). We thank the MAS at the University of Bath for help with collecting SEM micrographs. We thank David Apperley for collecting SS NMR data at the EPSRC-funded SS NMR facility at Durham University.

References

[1] S. L. Burkett, M. E. Davis, Structure-directing effects in the crown ether-mediated syntheses of FAU and EMT zeolites, Microporous Materials 1 (4) (1993) 265–282.

[2] T. Ohsuna, O. Terasaki, V. Alfredsson, J.-O. Bovin, D. Watanabe, S. W. Carr, M. W. Anderson, Observations on the role of crown ether templates in the formation of hexagonal and cubic polymorphs of zeolite Y, in: Proceedings of the Royal Society of London A: Mathematical, Physical and Engineering Sciences, Vol. 452, The Royal Society, 1996, pp. 715–740.

[3] A. Sartbaeva, S. A. Wells, M. Treacy, M. Thorpe, The flexibility window in zeolites, Nature materials 5 (12) (2006) 962–965.

[4] J. Newsam, M. Treacy, D. Vaughan, K. Strohmaier, W. Mortier, The structure of zeolite ZSM-20: mixed cubic and hexagonal stackings of faujasite sheets, Journal of the Chemical Society, Chemical Communications (8) (1989) 493–495.

[5] C. Baerlocher, L. B. McCusker, R. Chiappetta, Location of the 18-crown-6 template in EMC-2 (EMT) rietveld refinement of the calcined and as-synthesized forms, Microporous Materials 2 (4) (1994) 269–280.

[6] M. Treacy, D. Vaughan, K. Strohmaier, J. Newsam, Intergrowth segregation in FAU-EMT zeolite materials, in: Proceedings of the Royal Society of London A: Mathematical, Physical and Engineering Sciences, Vol. 452, The Royal Society, 1996, pp. 813–840.

[7] D. Vaughan, M. Treacy, J. Newsam, K. Strohmaier, W. Mortier, Synthesis and characterization of zeolite ZSM-20, 1989.

[8] F. Delprato, L. Delmotte, J. Guth, L. Huve, Synthesis of new silica-rich cubic and hexagonal faujasites using crown-etherbased supramolecules as templates, Zeolites 10 (6) (1990) 546–552.

[9] C. Baerlocher, L. B. McCusker, D. H. Olson, Atlas of zeolite framework types, Elsevier, 2007.

[10] M. M. Treacy, J. B. Higgins, Collection of simulated XRD powder patterns for zeolites fifth (5th) revised edition, Elsevier, 2007.

[11] C. Baerlocher, L. McCusker, Database of Zeolite Structures, `http://www.iza-structure.org/databases/`, [Online; accessed 23-November-2016] (2016).

[12] O. Terasaki, T. Ohsuna, V. Alfredsson, J. Bovin, D. Watanabe, S. W. Carr, M. W. Anderson, Observation of spatially correlated intergrowths of faujasitic polytypes and the pure end members by high-resolution electron microscopy, Chemistry of materials 5 (4) (1993) 452–458.

[13] E.-P. Ng, H. Awala, J.-P. Ghoy, A. Vicente, T. C. Ling, Y. H. Ng, S. Mintova, F. Adam, Effects of ultrasonic irradiation on crystallization and structural properties of EMT-type zeolite nanocrystals, Materials Chemistry and Physics 159 (2015) 38–45.

[14] E.-P. Ng, J.-M. Goupil, A. Vicente, C. Fernandez, R. Retoux, V. Valtchev, S. Mintova, Nucleation and crystal growth features of EMT-type zeolite synthesized from an organic-template-free system, Chemistry of Materials 24 (24) (2012) 4758–4765.

[15] E.-P. Ng, D. Chateigner, T. Bein, V. Valtchev, S. Mintova, Capturing ultrasmall EMT zeolite from template-free systems, Science 335 (6064) (2012) 70–73.

[16] K. M. Leung, P. P. Edwards, E. Jones, A. Sartbaeva, Microwave synthesis of LTN framework zeolite with no organic structure directing agents, RSC Advances 5 (45) (2015) 35580–35585.

[17] S. F. Mousavi, M. Jafari, M. Kazemimoghadam, T. Mohammadi, Template free crystallization of zeolite Rho via hydrothermal synthesis: Effects of synthesis time, synthesis temperature, water content and alkalinity, Ceramics International 39 (6) (2013) 7149–7158.

[18] J. Zhu, Z. Liu, A. Endo, Y. Yanaba, T. Yoshikawa, T. Wakihara, T. Okubo, Ultrafast, OSDA-free synthesis of mordenite zeolite, CrystEngComm 19 (4) (2017) 632–640.

[19] R. Wendelbo, M. Stöcker, H. Junggreen, H. B. Mostad, D. E. Akporiaye, Tumbling approach towards template-free synthesis of EMT zeolite, Microporous and mesoporous materials 28 (3) (1999) 361–375.

[20] E. Feijen, B. Matthijs, P. Grobet, J. Martens, P. Jacobs, Structure directing role of Na^+ and TMA^+ cations in 18-crown-6 ether mediated crystallization of EMT, MAZ and SOD aluminosilicate zeolites, Studies in Surface Science and Catalysis 105 (1997) 165–172.

[21] E. J. Feijen, K. De Vadder, M. H. Bosschaerts, J. L. Lievens, J. A. Martens, P. J. Grobet, P. A. Jacobs, Role of 18-crown-6 and 15-crown-5 ethers in the crystallization of polytype faujasite zeolites, Journal of the American Chemical Society 116 (7) (1994) 2950–2957.

[22] A. Nearchou, A. Sartbaeva, Influence of alkali metal cations on the formation of zeolites under hydrothermal conditions with no organic structure directing agents, CrystEngComm 17 (12) (2015) 2496–2503.

[23] H. Robson, Verified synthesis of zeolitic materials, Gulf Professional Publishing, 2001.

[24] T. Holland, S. Redfern, Unit cell refinement from powder diffraction data: the use of regression diagnostics, Mineralogical Magazine 61 (1) (1997) 65–77.

[25] R. E. Fletcher, S. A. Wells, K. M. Leung, P. P. Edwards, A. Sartbaeva, Intrinsic flexibility of porous materials; theory, modelling and the flexibility window of the EMT zeolite framework, Acta Crystallographica Section B: Structural Science, Crystal Engineering and Materials 71 (6) (2015) 641–647.

[26] J. Dhainaut, T. Daou, A. Chappaz, N. Bats, B. Harbuzaru, G. Lapisardi, H. Chaumeil, A. Defoin, L. Rouleau, J. Patarin, Synthesis of FAU and EMT-type zeolites using structure-directing agents specifically designed by molecular modelling, Microporous and Mesoporous Materials 174 (2013) 117–125.

[27] E. Lippmaa, M. Mägi, A. Samoson, M. Tarmak, G. Engelhardt, Investigation of the structure of zeolites by solid-state high-resolution silicon-29 NMR spectroscopy, Journal of the American Chemical Society 103 (17) (1981) 4992–4996.

[28] A. Sartbaeva, N. H. Rees, P. P. Edwards, A. J. Ramirez-Cuesta, E. Barney, Local probes show that framework modification in zeolites occurs on ammonium exchange without calcination, Journal of Materials Chemistry A 1 (25) (2013) 7415–7421.

[29] M. Hunger, G. Engelhardt, H. Koller, J. Weitkamp, Characterization of sodium cations in dehydrated faujasites and zeolite EMT by ^{23}Na DOR, 2D nutation, and MAS NMR, Solid state nuclear magnetic resonance 2 (3) (1993) 111–120.

[30] M. Feuerstein, M. Hunger, G. Engelhardt, J. Amoureux, Characterisation of sodium cations in dehydrated zeolite NaX by ^{23}Na NMR spectroscopy, Solid state nuclear magnetic resonance 7 (2) (1996) 95–103.